Real-space circuit complexity as a probe of phase diagrams

Nishan C. Jayarama [*]

Department of Physics, Indian Institute of Technology, Kanpur 208016, Uttar Pradesh, India

Viktor Svensson [†]

Division of Solid State Physics and NanoLund, Lund University, S-22100 Lund, Sweden

Circuit complexity has been used as a tool to study various properties in condensed matter systems, in particular as a way to probe the phase diagram. However, compared with measures based on entanglement, complexity has been found lacking. We show that when imposing penalty factors punishing nonlocality, it becomes a much stronger probe of the phase diagram, able to probe more subtle features. We do this by deriving analytical solutions for the complexity in the XY chain with transverse field.

I. INTRODUCTION AND OUTLINE

The borrowing of tools from quantum information science to study models in different areas of physics has been a fruitful undertaking, particularly in high-energy physics and condensed matter systems. One of these tools is the computational complexity—the minimum number of elementary operations to complete a given task. While initially applied to studies of algorithms, a geometric formulation of complexity [1–4] has in recent years found use in several other fields. In the anti–de Sitter and conformal field theory (AdS-CFT) correspondence [5], entanglement entropy is dual to the area of surfaces [6]. The proposal that complexity plays the role of something like a volume [7–12] has generated a lot of activity in defining and calculating new observables on both sides of the correspondence. Many papers have studied this on the quantum field theory side, developing the machinery and applying it to a variety of systems [13–26].

Independent of its role in holographic duality, a natural question is to what extent complexity can be used as a tool to probe the properties of different systems. For example, can complexity diagnose different phases or characterize quantum chaos? A number of works have shown this to be true [27–38].

Much of this work is made in the context of free-fermion models, where the optimal circuit implements a Bogoliubov rotation in momentum space. In the transverse field XY chain, the analytic properties of the complexity of these momentum-space circuits show signatures of phase transition [27,28]. There is another feature of the phase diagram, the red dashed curve in Fig. 1, called the factorizing curve. States along this curve factorize into a product state of the local spins and divide regions where correlation functions exhibit oscillatory behavior or not. It can be detected in measures based on

entanglement [39–42], but it was not seen in studies of circuit complexity.

These studies use a circuit based on Bogoliubov rotations in momentum space, which is inherently nonlocal. A fully local treatment would start with some set of local gates, such as nearest-neighbor hoppings and pairings, and construct an optimal circuit out of these. This notion can be used to classify topological phases [43], but deriving explicit circuits and the complexity is a hard problem.

In this paper, we pursue another strategy of including the effects of locality on circuit complexity. We reinterpret the Bogoliubov circuit as a real-space circuit, thereby changing the cost function and enabling the use of penalty factors as a way of punishing nonlocality. The simpler problem that we attack can be solved analytically but still allows us to uncover some interesting features that we expect to show up in a fully local treatment. With these penalty factors, complexity is sensitive to more subtle features of the phase diagram, and the factorizing curve can be detected. Section II contains a quick introduction to the model and the Bogoliubov circuits that connect different ground states. In Sec. III we derive the momentum-space complexity, followed by the real-space complexity in Sec. IV. Section V shows how penalty factors enable us to detect more features of the phase diagram. Section VI concerns the scaling limit close to the phase transition.

II. SETUP

The Hamiltonian for the XY chain is given by

$$H = -\frac{1}{2}\sum_{j=1}^{N}\left[\left(\frac{1+\gamma}{2}\right)\sigma_j^x\sigma_{j+1}^x + \left(\frac{1-\gamma}{2}\right)\sigma_j^y\sigma_{j+1}^y + h\sigma_j^z\right]. \tag{1}$$

Following the procedure in Ref. [44], the Hamiltonian can be diagonalized by a Jordan-Wigner transformation giving

$$H = h\sum_{j=1}^{N}\psi_j^\dagger\psi_j - \frac{1}{2}\sum_{j=1}^{N-1}(\psi_j^\dagger\psi_{j+1} + \gamma\psi_j^\dagger\psi_{j+1}^\dagger + \text{H.c.}) \tag{2}$$

[*]nishancj@iitk.ac.in
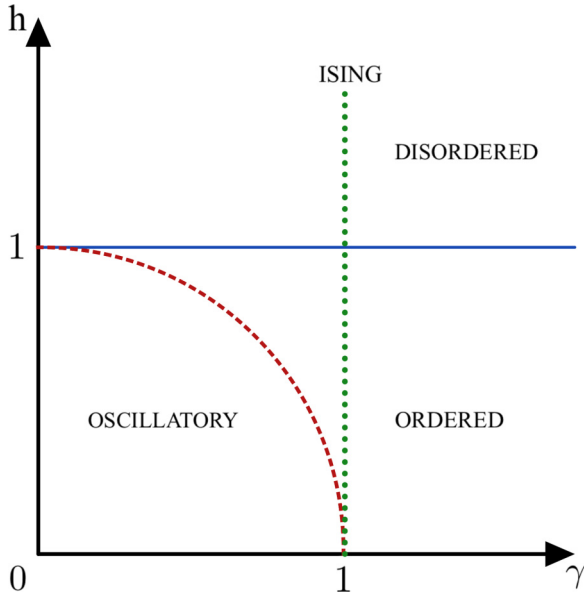
[†]viktor.svensson@ftf.lth.se

FIG. 1. Phase diagram of the XY chain.

followed by a Bogoliubov rotation to give

$$H = \frac{1}{N} \sum_{q \in \Gamma} \epsilon(q) \chi_q^\dagger \chi_q, \tag{3}$$

where $\epsilon(q) = \sqrt{(h - \cos q)^2 + (\gamma \sin q)^2}$ and $\Gamma = \frac{2\pi}{N}(-\frac{N-1}{2}, -\frac{N-1}{2} + 1, \ldots, \frac{N-1}{2})$. We have removed irrelevant energy shifts and boundary terms as we will always work in the large-N limit.

The phase diagram of this model is shown in Fig. 1. We will study the complexity of connecting the ground states of Hamiltonians with different parameters. We define (γ_R, h_R) and (γ_T, h_T) to be the parameters corresponding to the reference and target states. A unitary transformation that accomplishes this is

$$U = \prod_{q>0, q \in \Gamma} U_q = \exp\left[\sum_{q>0, q \in \Gamma} (v_q^T - v_q^R) A_q \right], \tag{4}$$

where

$$A_q = \frac{1}{N}(\chi_q^\dagger \chi_{-q}^\dagger + \chi_q \chi_{-q}), \tag{5}$$

$$v_q = \frac{1}{2} \arctan\left(\frac{\gamma \sin q}{h - \cos q} \right). \tag{6}$$

The fermions in A_q can be chosen to be the Bogoliubov fermions of any state, as the functional form is invariant under Bogoliubov rotations.

In the following sections, we will evaluate the circuit complexity for different circuits, both in momentum space and in real space. We will choose the reference and target states as ground states of the XY chain.

III. MOMENTUM-SPACE COMPLEXITY

Because the different sectors q are decoupled, we may consider them separately. Following Nielsen's geometric approach, we write the unitary as the end point of a path-ordered exponential

$$U_q(s) = \overleftarrow{\mathcal{P}} \exp\left(\int_0^s ds' Y(s) A_q \right), \tag{7}$$

such that $U_q(0) = \mathbb{1}$ and $U_q(1) = U_q$. We define the circuit depth as

$$\mathcal{D}[U_q] = \int_0^1 ds |Y(s)|^2, \tag{8}$$

and to find the complexity $\mathcal{C}_q$, we minimize this quantity with respect to Y. The complexity is simply

$$\mathcal{C}_q = |\Delta v_q|^2. \tag{9}$$

The complexity for the full unitary is then the sum over each momentum mode:

$$\mathcal{C} = \sum_q \mathcal{C}_q = \sum_q \left| v_q^R - v_q^T \right|^2. \tag{10}$$

When the system size goes to infinity, this is amenable to analytic treatment, but we save this treatment for the real-space complexity in the next section. By Parseval's theorem, the momentum-space complexity is a special case of the real-space one.

IV. REAL-SPACE COMPLEXITY

A. Transforming the circuit

In this section, we reinterpret the momentum-space circuit as a real-space circuit. We define the real-space complexity including penalty factors and analytically solve for the complexity. We use the same unitary, but through a Bogoliubov rotation and Fourier transform we can express it in terms of the original fermions as

$$U = \prod_{n=1}^{N-1} U_n = \prod_{n=1}^{N-1} \exp[K_n G_n], \tag{11}$$

where

$$K_n = \frac{2i}{N} \sum_{q>0, q \in \Gamma} \Delta v_q \sin(qn), \tag{12}$$

$$G_n = \sum_{j=1}^{N} i(\psi_{j+n}^\dagger \psi_j^\dagger - \psi_j \psi_{j+n}); \tag{13}$$

see Appendix A for more details. The unitary effectively decouples different values of n, and thus the complexity of the unitary will be the sum of the complexity of unitaries corresponding to each n mode.

B. Complexity

We consider a path-ordered exponential of the form

$$U_n(s) = \overleftarrow{\mathcal{P}} \exp\left(\int_0^s ds' \bar{Y}_n(s) G_n \right). \tag{14}$$

The circuit depth is

$$\mathcal{D}[U_n] = \int_0^1 e^{nl} n^\beta |\bar{Y}_n(s)|^2 ds, \qquad (15)$$

where we include penalty factors l and β. When these penalty factors are greater than zero, they punish the use of nonlocal gates. The complexity for this mode is $\mathcal{C}_n = e^{nl} n^\beta |K_n|^2$ (see Appendix B for the full derivation), and the full complexity is just the sum

$$\mathcal{C} = \sum_{n=1}^{N-1} e^{2nl} n^\beta |K_n|^2. \qquad (16)$$

We evaluate (16) in the infinite-system-size limit where

$$I_n = \frac{2i}{N} \sum_{q>0, q\in\Gamma} v_q \sin(qn) \rightarrow \int_{-\pi}^{\pi} e^{iqn} v_q dq. \qquad (17)$$

One can evaluate the above integral using contour integration techniques [27,44]. The answer to the integral is dependent on which phase we are in, and the details are shown in Appendix C. In the disordered (D) and ordered (O) phases we have

$$I_n^{(D)} = \frac{i\pi}{2n}(\lambda_-^n - \lambda_+^{-n}), \qquad (18)$$

$$I_n^{(O)} = \frac{i\pi}{2n}(2 - \lambda_+^n - \lambda_-^n), \qquad (19)$$

respectively, where

$$\lambda_\pm = \frac{h \pm \sqrt{h^2 + \gamma^2 - 1}}{1 + \gamma}. \qquad (20)$$

These parameters are connected to the correlation lengths $\xi_\pm$ as

$$\xi_\pm = \frac{1}{|\ln \lambda_\pm|}. \qquad (21)$$

The final result is

$$\mathcal{C} = \sum_{n=1}^{\infty} e^{2nl} n^\beta |I_n^T - I_n^R|^2, \qquad (22)$$

where one uses $I^{(O)}$ or $I^{(D)}$ depending on where the target and reference state are located. This sum can be performed and takes the schematic form

$$\mathcal{C} = \sum_{i,j} \pm \text{PolyLog}(2 - \beta, \lambda_i \lambda_j e^{2l}), \qquad (23)$$

where we sum over those λ which are contained in the unit circle. Note that this formula can also be used outside the radius of convergence of the sum in (16), where it represents an analytic continuation. However, it *should not* be used there, since the sum is the correct representation of the effort in constructing the circuit.

V. THE EFFECT OF PENALTY FACTORS

In this section, we will study the influence of the penalty factors l and β, which both punish the use of long gates. The
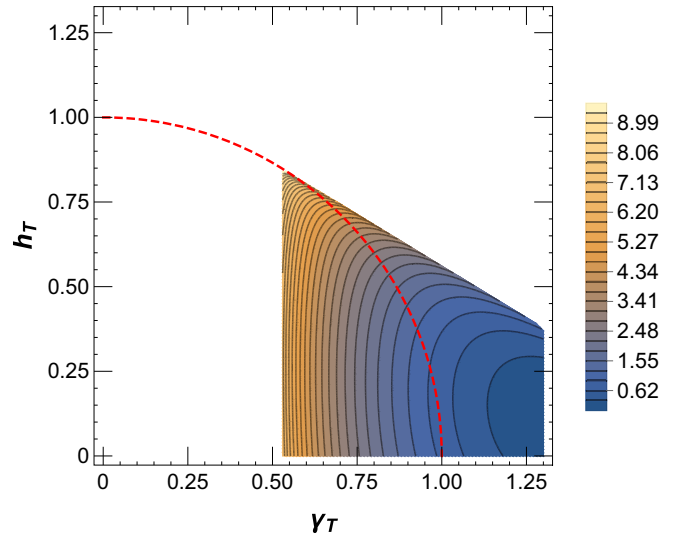

FIG. 2. A contour plot of $\mathcal{C}$ as a function of h_T and γ_T with the parameters $l = |\ln 0.56| = 0.58$, $h_R = 0.1$, $\gamma_R = 1.4$, $\beta = 0$. The red dashed semicircle is the factorizing curve. Complexity diverges in the white regions.

essential difference is that one of them introduces a length scale, while the other is scale invariant. As a result, they have very different effects. For this section, we will assume that our reference state is in the ordered phase and far away from the phase transition. The case without penalty factors, $l = \beta = 0$, is equivalent to the momentum-space case by Parseval's theorem.

The penalty factor e^{2nl} penalizes the use of gates of length scales greater than $1/l$. When the correlation length of the target state exceeds this length scale, we should expect the complexity to be large. In fact, the radius of convergence of the sum in (16) is exactly where $l\xi = 1$. Beyond this point, the complexity is infinite. We see this explicitly in Fig. 2, which shows the complexity for a nonzero value of l. The dashed curve is the factorizing curve, and we note that the boundary features a sharp kink along this curve. For a given choice of l, the curve where $l\xi = 1$ divides states that are accessible from those that are not. This follows from the fact that the radius of convergence of the second argument in the PolyLog is 1. We show these curves in a contour plot of λ in Fig. 3. From this perspective, the appearance of the factorizing curve has a clear explanation. λ is complex within the circle but real outside of it. Switching from one to the other entails a collision with the other root in Eq. (20), a nonanalytic process that gives rise to the sharp feature in the plot. By introducing a penalty factor with a length scale, complexity becomes sensitive to this feature as the radius of convergence will lie along a contour of Fig. 3. Note that one needs to vary l from 0 to ∞ in order to reproduce the full curve using complexity.

We now come to n^β. This penalty factor also penalizes the use of circuits with constituent gates of long length, but does not introduce a new length scale. A natural choice that models the case where circuit are built from local gates is $\beta = 1$. To see this, note that the gates we use, G_n, are built from fermions acting n sites apart. One needs at least n local gates to construct it, corresponding to $\beta = 1$.
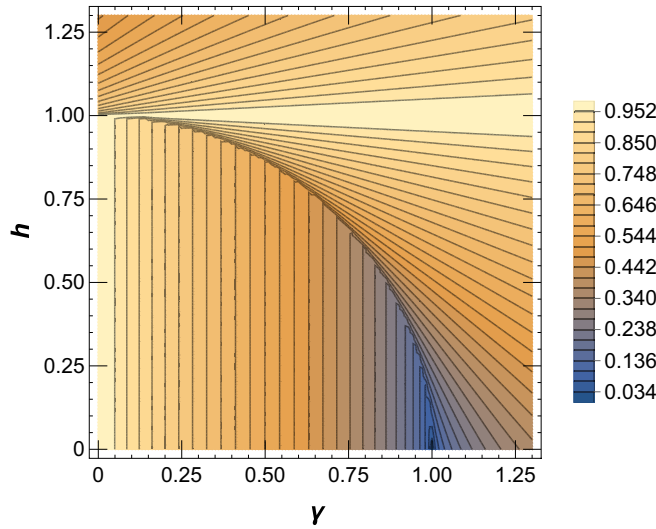
FIG. 3. A contour plot of the relevant correlation parameters: $|\lambda_+|$ in the ordered phase and $|\lambda_+^{-1}|$ in the disordered phase as a function of h and γ. Note that the "oscillatory" phase is visible in this plot.

The consequence of this penalty factor close to the phase transition is shown in Fig. 4. As β is increased, the behavior at the phase transition becomes sharper. At $\beta = 1$, the complexity diverges at the transition. This matches the intuition that it takes an infinite number of local gates to reach the phase transition where the correlation length diverges. This is a complementary perspective to the momentum-space picture where nonanalyticities are interpreted as a consequence of the change in winding number [27].

VI. SCALINGS AT THE PHASE TRANSITION

In this section, we show analytic results for how complexity scales as the target state approaches the phase transition. We choose the reference state in the ordered phase far from the phase transition, $h_T = 1 - \epsilon$ and $\gamma_T \neq 0$. We keep $l = 0$, as otherwise the phase transition is unreachable. The form of the scaling depends on whether β is an integer less than or equal to 1 or not. The leading ϵ-dependent terms in the
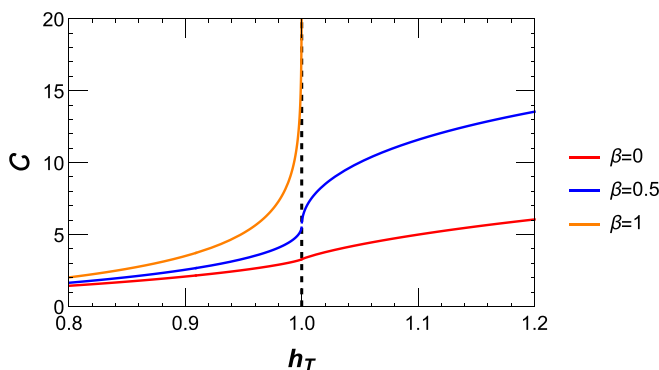

FIG. 4. Circuit complexity as a function of h_T for different values of β with the parameters $h_R = 0.1$, $\gamma_R = 1.1$, $\gamma_T = 1.1$, $l = 0$. β influences the analytic properties at the phase transition.

relevant cases are

$$\mathcal{C}_{\beta=0} \sim -\frac{\pi^2}{2\gamma_T} \epsilon \ln \epsilon, \tag{24}$$

$$\mathcal{C}_{\beta=1} \sim -\frac{\pi^2}{4} \ln \epsilon, \tag{25}$$

$$\mathcal{C}_{\beta \notin \mathbb{Z}} \sim \frac{\pi^2}{2^{1+\beta}\gamma_T^{1-\beta}} \Gamma(\beta - 1)\epsilon^{1-\beta}. \tag{26}$$

When $\beta = 0$, we see that $\mathcal{C}$ is finite, but its derivative $\frac{\partial \mathcal{C}}{\partial h_T}$ diverges as $\ln \epsilon$, as has been noted before [27,28,30,31]. For $\beta \geqslant 1$, the complexity itself is a divergent quantity, as seen in Fig. 4. We can interpret this in terms of the correlation length, which diverges as ϵ^{-1}. If the cost of a gate is proportional to its length, and the correlation length of the system diverges, so does the complexity. Apart from the case $\beta = 1$, the coefficient must contain an energy scale to balance out the powers of ϵ. This energy scale is set by γ_T, which determines the anisotropy of the spin chain. We also note that this leading term is independent of the reference state, whose influence only shows up at subleading orders in the expansion.

VII. CONCLUSION

We have reinterpreted the Bogoliubov circuits as real-space circuits. This enabled us to study the effects of penalty factors that punish the use of nonlocal gates. Because of the simplicity of the circuit, we are able to find analytical results for the complexity even including penalty factors.

Our main result is that the complexity is sensitive to the factorizing curve in the XY model if penalty factors are included. This is evident in Figs. 2 and 3. The physical reason is also clear from the analytical solution. By introducing a penalty factor with a length scale, we are able to probe the behavior of the correlation lengths of the system. These correlation lengths have a sharp change in behavior at this curve, where they collide and develop an imaginary part; see Eq. (20).

The other penalty factor, β, influences how the complexity behaves at the phase transition. At $\beta = 0$, only the derivative of the complexity diverges, as noted in previous papers. With the choice $\beta = 1$, which we argue models the case where the circuit is built from local gates, the complexity diverges. We show this numerically as well as analytically.

Our results follow mainly from the nonanalytic structure of the Bogoliubov angle, not from the precise form of the cost function. Our results will be robust under certain modifications of the cost function, such as changing L^2 to another norm L^p, since this change would not introduce any new nonanalyticities.

These findings show that including effects of locality, complexity is a more sensitive probe of the system than the momentum-space formulation based on Bogoliubov circuits. We expect that the same should hold for a fully local formulation of complexity where the circuit is built from local gates.

ACKNOWLEDGMENTS

APPENDIX A: FOURIER TRANSFORMING THE BOGOLIUBOV CIRCUIT

Here we show how to reinterpret the Bogoliubov circuit

$$U = \prod_{q>0, q\in\Gamma} U_q = \exp\left[\sum_{q>0, q\in\Gamma} (v_q^T - v_q^R)A_q\right] \quad (A1)$$

as a real-space circuit. As a first step, we write the circuit in terms of the original momentum-space fermions

$$U = \exp\left[\sum_{q>0, q\in\Gamma} \frac{\Delta v_q}{N}(\psi_q^\dagger \psi_{-q}^\dagger + \psi_q \psi_{-q})\right]. \quad (A2)$$

Now we rewrite the operator in the exponent in terms of the real-space fermions

$$\psi_q^\dagger \psi_{-q}^\dagger + \psi_q \psi_{-q} = i \sum_{j,k=1}^{N} \left(e^{iq(j-k)}\psi_j^\dagger \psi_k^\dagger + e^{-iq(j-k)}\psi_k \psi_j\right). \quad (A3)$$

We can rearrange the sum by defining $(j-k) = n$ as a new variable

$$\psi_q^\dagger \psi_{-q}^\dagger + \psi_q \psi_{-q} = i \sum_{j=1}^{N} \sum_{n=1-N}^{(N-1)} (e^{iqn}\psi_{j+n}^\dagger \psi_j^\dagger + e^{-iqn}\psi_j \psi_{j+n}). \quad (A4)$$

Rewriting $e^{iqn} = \cos(qn) + i\sin(qn)$, we can rewrite the above sum as

$$\psi_q^\dagger \psi_{-q}^\dagger + \psi_q \psi_{-q} = i \sum_{n=-(N-1)}^{(N-1)} [\cos(qn)H_n + \sin(qn)G_n], \quad (A5)$$

where we have defined two new Hermitian gates H_n and G_n as

$$H_n = \sum_{j=1}^{N}(\psi_{j+n}^\dagger \psi_j^\dagger + \psi_j \psi_{j+n}), \quad (A6)$$

$$G_n = \sum_{j=1}^{N} i(\psi_{j+n}^\dagger \psi_j^\dagger - \psi_j \psi_{j+n}). \quad (A7)$$

By noticing that H_n and G_n are odd in n, it can be inferred that

$$\sum_{n=-(N-1)}^{(N-1)} \cos(qn)H_n = 0. \quad (A8)$$

Plugging Eq. (A4) into Eq. (A2), we find that the unitary connecting ground states can now be written as

$$U = \exp\left[\sum_{n=1}^{N-1} K_n G_n\right], \quad (A9)$$

where $K_n = \frac{2i}{N}\sum_{q>0, q\in\Gamma} \Delta v_q \sin(qn)$. It can be shown that

$$[G_n, G_{n'}] = 0, \quad (A10)$$

and so the unitary can be factorized as

$$U = \prod_{n=1}^{N-1} U_n = \prod_{n=1}^{N-1} \exp[K_n G_n]. \quad (A11)$$

APPENDIX B: ANALYTIC DERIVATION OF COMPLEXITY

In this Appendix, we derive an analytical formula for the real-space circuit complexity using Nielsen's formulation, closely following a similar derivation in Sec. 2.1 of Ref. [18]. We first construct the circuit for a given n mode and define the complexity for the same. We can construct the required unitary using a path-ordered exponential of the form

$$U_n(s) = \overleftarrow{\mathcal{P}} \exp\left(\int_0^s ds' \bar{Y}_n(s)G_n\right). \quad (B1)$$

We can obtain the control functions $\bar{Y}_n(s)$ using the tangent equation

$$\frac{\partial U_s}{\partial s}U_s^{-1} = \bar{Y}_n(s)G_n. \quad (B2)$$

We minimize the circuit depth for this given unitary to obtain the optimal circuit. It is given by

$$\mathcal{D}[U_n] = \int_0^1 ds |\bar{Y}_n(s)|^2. \quad (B3)$$

We consider a circuit unitary ansatz of the form

$$U_n(s) = \exp[a_n(s)G_n]. \quad (B4)$$

This unitary can be used to build up the unitary that connects the ground states with the boundary conditions $a_n(0) = 0$ and $a_n(1) = K_n$. Plugging the ansatz into (B2),

$$\bar{Y}_n(s) = \dot{a}_n(s). \quad (B5)$$

The circuit depth of this unitary is given by

$$\mathcal{D}[U_n] = \int_0^1 ds |\dot{a}_n(s)|^2. \quad (B6)$$

We can minimize this depth by treating it as an action and extremizing it. The corresponding Euler-Lagrange equation for a_n is given by

$$\ddot{a}_n = 0. \quad (B7)$$

On solving the above equation with the appropriate boundary conditions, we obtain

$$a_n(s) = sK_n. \quad (B8)$$

Hence the complexity of a single n mode is given by

$$\mathcal{C}_n = \min(\mathcal{D}[U_n]) = |K_n|^2. \quad (B9)$$

The complexity for the complete unitary will just be the sum of the complexities for each n mode. We can also introduce the penalty factors at this stage and write the total complexity as

$$\mathcal{C} = \sum_{n=1}^{N-1} e^{2nl}n^\beta \mathcal{C}_n = \sum_{n=1}^{N-1} e^{2nl}n^\beta |K_n|^2. \quad (B10)$$
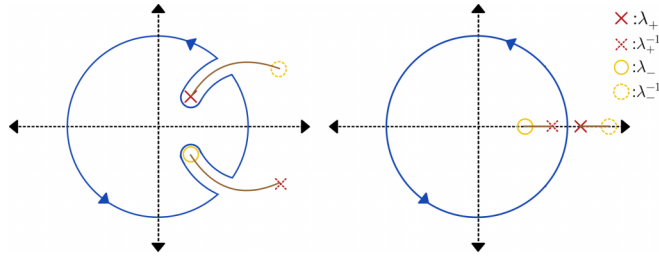
FIG. 5. A complex plot showing the integration contour ($|t| = 1$) in blue used to calculate the Fourier transform of v_q. The brown lines denote branch cuts. In the left panel, the branch cut touches the integration contour at the points z and $\bar{z}$. The contour in the left panel is used for states which are in the ordered phase (within the oscillatory phase to be precise, but the branch cut leaves the contour in the same way for states outside the oscillatory phase but within the ordered phase, in which case λ_+ and λ_-^{-1} move to the real line). The contour in the right panel is used for states in the disordered phase. As the contour completely surrounds the branch cut, one can deform it to be around the branch points within to simplify the integral.

APPENDIX C: FOURIER INTEGRAL OF v_q

To evaluate an explicit expression for the real-space complexity, we are required to evaluate integrals of the form

$$I_n = \int_{-\pi}^{\pi} e^{iqn} v_q \, dq. \tag{C1}$$

Making the change of variable $t = e^{iq}$, we have

$$\frac{i}{2} \oint_{|t|=1} t^{n-1} \arctan\left[\frac{i\gamma(t^2 - 1)}{-2ht + t^2 + 1}\right] dt. \tag{C2}$$

Rewriting the arctan in terms of logarithms, we have

$$\frac{-1}{4} \oint_{|t|=1} t^{n-1} \ln\left[\frac{\gamma + 2ht - (\gamma + 1)t^2 - 1}{-\gamma + 2ht + (\gamma - 1)t^2 - 1}\right] dt. \tag{C3}$$

One can evaluate the above integral using contour integration techniques, with the contour shown in Fig. 5. The answer will be in the form of the natural length parameters of the spin chain, given by

$$\lambda_{\pm} = \frac{h \pm \sqrt{h^2 + \gamma^2 - 1}}{1 + \gamma}. \tag{C4}$$

We can rewrite the integral in terms of these λ's as

$$\frac{1}{4} \oint_{|t|=1} t^{n-1} f_\lambda(t) \, dt$$

$$= \frac{1}{4} \oint_{|t|=1} t^{n-1} \ln\left[\frac{\left(t - \left(\frac{1}{\lambda}\right)_+\right)\left(t - \left(\frac{1}{\lambda}\right)_-\right)}{(t - \lambda_+)(t - \lambda_-)}\right] dt. \tag{C5}$$

The answer to (C5) will depend on which phase we are in. Studying the branch cut structure of $f_\lambda(t)$ will help us solve the integral.
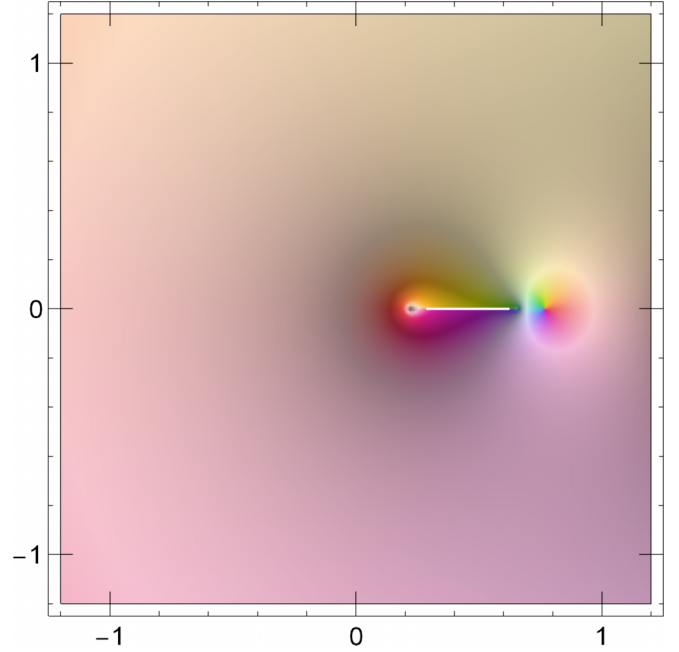

FIG. 6. A complex plot of $f_\lambda(t)$ with $h \to 1.3$, $\gamma \to 0.5$, which is in the disordered phase. The white line in the plot is a branch cut that connects λ_- on the left to λ_+^{-1} on the right. On crossing the branch cut from the magenta side to the green side, one picks up a constant piece of $2\pi i$ due to the logarithm.

1. Disordered phase

In the disordered phase (see right panel of Fig. 5, as well as Fig. 6), the branch cut is completely contained within the unit contour; we can deform the contour to be around the branch cut and solve the contour integral. The contour that goes around the branch point goes to zero as there is no pole, and we are only left with the integrals above and below the branch cut

$$\frac{1}{4} \oint_{|t|=1} t^{n-1} f_\lambda(t) \, dt$$

$$= \frac{1}{4}\left[\int_{\lambda_+^{-1}}^{\lambda_-} t^{n-1}(2\pi i + f_\lambda(t)) \, dt + \int_{\lambda_-}^{\lambda_+^{-1}} t^{n-1} f_\lambda(t) \, dt\right]$$

$$= \frac{i\pi}{2} \int_{\lambda_+^{-1}}^{\lambda_-} t^{n-1} \, dt. \tag{C6}$$

Thus, in the disordered phase,

$$I_n = \frac{1}{4} \oint_{|t|=1} t^{n-1} f_\lambda(t) \, dt = \frac{i\pi}{2}\left(\frac{\lambda_-^n}{n} - \frac{\lambda_+^{-n}}{n}\right). \tag{C7}$$

2. Ordered phase

In the ordered phase (see left panel of Fig. 5, as well as Fig. 7), the branch cuts move out of the unit contour, and we will denote the point at which the branch cut crosses the unit circle in the top half plane as z. We can use the inherent mirror symmetry to come to the conclusion that $\bar{z}$ will be the point at which the branch cut crosses the unit circle in the lower half
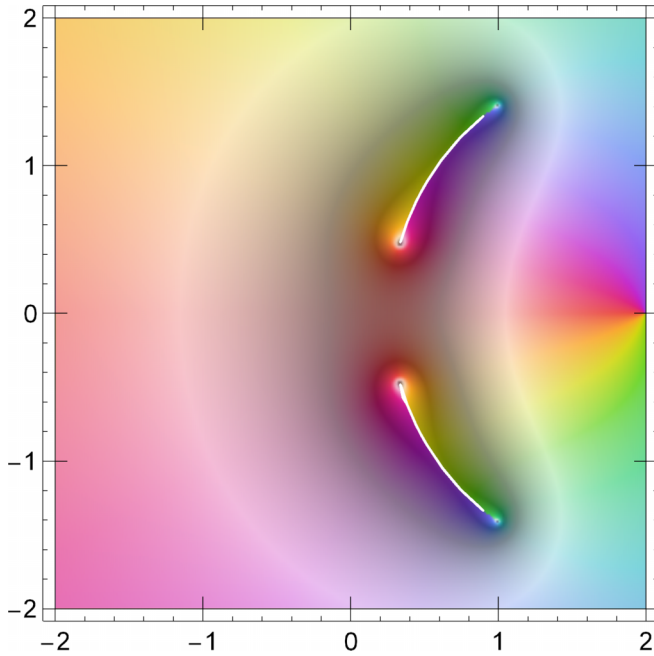
FIG. 7. A complex plot of $f_\lambda(t)$ with $h \to 0.5$, $\gamma \to 0.5$, which is in the ordered phase. The white curves in the plot are branch cuts, one of which connects λ_+ on the left to λ_-^{-1} on the right (top half) and one of which connects λ_- on the left to λ_+^{-1} on the right (bottom half). On crossing the branch cuts from the magenta side to the green side, one picks up a constant piece of $2\pi i$ due to the logarithm.

plane. In such a case, we would need to deform our contour as shown in the left panel of Fig. 5. Once again, the integrals

around the branch points will turn out to be zero, and we are left with the integrals above and below the branch cuts

$$
\frac{1}{4} \oint_{|t|=1} t^{n-1} f_\lambda(t) dt = \frac{1}{4} \left[\int_{\lambda_+}^{z} t^{n-1}(2\pi i + f_\lambda(t)) dt \right.
$$
$$
+ \int_{z}^{\lambda_+} t^{n-1} f_\lambda(t) dt + \int_{\lambda_-}^{\bar{z}} t^{n-1}(2\pi i + f_\lambda(t)) dt
$$
$$
\left. + \int_{\bar{z}}^{\lambda_-} t^{n-1} f_\lambda(t) dt \right]. \tag{C8}
$$

This integral simplifies to

$$
\frac{1}{4} \oint_{|t|=1} t^{n-1} f_\lambda(t) dt = \frac{i\pi}{2} \int_{\lambda_+}^{z} t^{n-1} dt + \frac{i\pi}{2} \int_{\lambda_-}^{\bar{z}} t^{n-1} dt. \tag{C9}
$$

Thus, in the ordered phase,

$$
I_n = \frac{i\pi}{2} \left(\frac{z^n}{n} + \frac{\bar{z}^n}{n} - \frac{\lambda_+^n}{n} - \frac{\lambda_-^n}{n} \right). \tag{C10}
$$

Since z is on the unit circle, we can take $z \to e^{i\theta}$ and rewrite I_n as

$$
I_n = \frac{i\pi}{2} \left(\frac{e^{in\theta}}{n} + \frac{e^{-in\theta}}{n} - \frac{\lambda_+^n}{n} - \frac{\lambda_-^n}{n} \right). \tag{C11}
$$

While we have put the two branch cuts at θ and $-\theta$, in order to get a correct circuit, they need to coincide. At a branch cut, the Bogoliubov angle jumps by $\pi/2$. However, the circuit is only invariant (up to a sign) under shifts by π, and so these two shifts have to happen at the same point. Therefore we put $\theta = 0$.

[1] M. A. Nielsen, A geometric approach to quantum circuit lower bounds, Quantum Inf. Comput. **6**, 213 (2006).

[2] M. A. Nielsen, M. R. Dowling, M. Gu, and A. C. Doherty, Quantum computation as geometry, Science **311**, 1133 (2006).

[3] M. R. Dowling and M. A. Nielsen, The geometry of quantum computation, Quantum Inf. Comput. **8**, 0861 (2008).

[4] M. A. Nielsen, M. R. Dowling, M. Gu, and A. C. Doherty, Optimal control, geometry, and quantum computing, Phys. Rev. A **73**, 062323 (2006).

[5] J. M. Maldacena, The large-N limit of superconformal field theories and supergravity, Int. J. Theor. Phys. **38**, 1113 (1999).

[6] S. Ryu and T. Takayanagi, Holographic Derivation of Entanglement Entropy from AdS/CFT, Phys. Rev. Lett. **96**, 181602 (2006).

[7] L. Susskind, Entanglement is not enough, Fortschr. Phys. **64**, 49 (2016).

[8] L. Susskind, Computational complexity and black hole horizons, Fortschr. Phys. **64**, 24 (2016).

[9] L. Susskind, Addendum to computational complexity and black hole horizons, Fortschr. Phys. **64**, 44 (2016).

[10] D. Stanford and L. Susskind, Complexity and shock wave geometries, Phys. Rev. D **90**, 126007 (2014).

[11] A. R. Brown, D. A. Roberts, L. Susskind, B. Swingle, and Y. Zhao, Complexity, action, and black holes, Phys. Rev. D **93**, 086006 (2016).

[12] A. R. Brown, D. A. Roberts, L. Susskind, B. Swingle, and Y. Zhao, Complexity Equals Action, Phys. Rev. Lett. **116**, 191301 (2016).

[13] S. Chapman, M. P. Heller, H. Marrochio, and F. Pastawski, Toward a Definition of Complexity for Quantum Field Theory States, Phys. Rev. Lett. **120**, 121602 (2018).

[14] R. Jefferson and R. C. Myers, Circuit complexity in quantum field theory, J. High Energy Phys. 10 (2017) 107.

[15] R.-Q. Yang, Complexity for quantum field theory states and applications to thermofield double states, Phys. Rev. D **97**, 066004 (2018).

[16] M. Guo, J. Hernandez, R. C. Myers, and S.-M. Ruan, Circuit complexity for coherent states, J. High Energy Phys. 10 (2018) 011.

[17] D. W. F. Alves and G. Camilo, Evolution of complexity following a quantum quench in free field theory, J. High Energy Phys. 06 (2018) 029.

[18] S. Chapman, J. Eisert, L. Hackl, M. P. Heller, R. Jefferson, H. Marrochio, and R. Myers, Complexity and entanglement for thermofield double states, SciPost Phys. **6**, 034 (2019).

[19] L. Hackl and R. C. Myers, Circuit complexity for free fermions, J. High Energy Phys. 07 (2018) 139.

[20] R. Khan, C. Krishnan, and S. Sharma, Circuit complexity in fermionic field theory, Phys. Rev. D **98**, 126001 (2018).

[21] J. Jiang, J. Shan, and J.-Z. Yang, Circuit complexity for free fermion with a mass quench, Nucl. Phys. B **954**, 114988 (2020).

[22] R.-Q. Yang, Y.-S. An, C. Niu, C.-Y. Zhang, and K.-Y. Kim, Principles and symmetries of complexity in quantum field theory, Eur. Phys. J. C **79**, 109 (2019).

[23] R.-Q. Yang, Y.-S. An, C. Niu, C.-Y. Zhang, and K.-Y. Kim, More on complexity of operators in quantum field theory, J. High Energy Phys. 03 (2019) 161.

[24] R.-Q. Yang and K.-Y. Kim, Complexity of operators generated by quantum mechanical Hamiltonians, J. High Energy Phys. 03 (2019) 010.

[25] M. Flory and M. P. Heller, Geometry of complexity in conformal field theory, Phys. Rev. Res. **2**, 043438 (2020).

[26] A. P. Reynolds and S. F. Ross, Complexity of the AdS soliton, Classical Quantum Gravity **35**, 095006 (2018).

[27] F. Liu, S. Whitsitt, J. B. Curtis, R. Lundgren, P. Titum, Z.-C. Yang, J. R. Garrison, and A. V. Gorshkov, Circuit complexity across a topological phase transition, Phys. Rev. Res. **2**, 013323 (2020).

[28] Z. Xiong, D.-X. Yao, and Z. Yan, Nonanalyticity of circuit complexity across topological phase transitions, Phys. Rev. B **101**, 174305 (2020).

[29] T. Ali, A. Bhattacharyya, S. Shajidul Haque, E. H. Kim, and N. Moynihan, Post-quench evolution of complexity and entanglement in a topological system, Phys. Lett. B **811**, 135919 (2020).

[30] N. Jaiswal, M. Gautam, and T. Sarkar, Complexity and information geometry in the transverse *XY* model, Phys. Rev. E **104**, 024127 (2021).

[31] N. Jaiswal, M. Gautam, and T. Sarkar, Complexity, information geometry, and Loschmidt echo near quantum criticality, J. Stat. Mech. (2022) 073105.

[32] K. Pal, K. Pal, A. Gill, and T. Sarkar, Evolution of circuit complexity in a harmonic chain under multiple quenches, arXiv:2206.03366 [quant-ph].

[33] K. Pal, K. Pal, and T. Sarkar, Complexity in the Lipkin-Meshkov-Glick model, arXiv:2204.06354 [quant-ph].

[34] T. Ali, A. Bhattacharyya, S. S. Haque, E. H. Kim, N. Moynihan, and J. Murugan, Chaos and complexity in quantum mechanics, Phys. Rev. D **101**, 026021 (2020).

[35] H. A. Camargo, P. Caputa, D. Das, M. P. Heller, and R. Jefferson, Complexity as a Novel Probe of Quantum Quenches: Universal Scalings and Purifications, Phys. Rev. Lett. **122**, 081601 (2019).

[36] A. Bhattacharyya, A. Shekar, and A. Sinha, Circuit complexity in interacting QFTs and RG flows, J. High Energy Phys. 10 (2018) 140.

[37] V. Balasubramanian, M. DeCross, A. Kar, and O. Parrikar, Quantum complexity of time evolution with chaotic Hamiltonians, J. High Energy Phys. 01 (2020) 134.

[38] R.-Q. Yang and K.-Y. Kim, Time evolution of the complexity in chaotic systems: Concrete examples, J. High Energy Phys. 05 (2020) 045.

[39] T.-C. Wei, D. Das, S. Mukhopadyay, S. Vishveshwara, and P. M. Goldbart, Global entanglement and quantum criticality in spin chains, Phys. Rev. A **71**, 060305(R) (2005).

[40] L. Amico, F. Baroni, A. Fubini, D. Patane', V. Tognetti, and P. Verrucchi, Divergence of the entanglement range in low dimensional quantum systems, Phys. Rev. A **74**, 022322 (2006).

[41] S. M. Giampaolo, S. Montangero, F. Dell'Anno, S. De Siena, and F. Illuminati, Universal aspects in the behavior of the entanglement spectrum in one dimension: Scaling transition at the factorization point and ordered entangled structures, Phys. Rev. B **88**, 125142 (2013).

[42] G. Y. Chitov, K. Gadge, and P. N. Timonin, Disentanglement, disorder lines, and Majorana edge states in a solvable quantum chain, Phys. Rev. B **106**, 125146 (2022).

[43] X. Chen, Z.-C. Gu, and X.-G. Wen, Local unitary transformation, long-range quantum entanglement, wave function renormalization, and topological order, Phys. Rev. B **82**, 155138 (2010).

[44] F. Franchini, *An Introduction to Integrable Techniques for One-Dimensional Quantum Systems*, Lecture Notes in Physics Vol. 940 (Springer, New York, 2017).